Available online at www.sciencedirect.com
ScienceDirect
Journal of Power Sources 159 (2006) 1440–1449
JOURNAL OF POWER SOURCES
www.elsevier.com/locate/jpowsour

Optimization of electrode paste composition and structure for improving energy and life characteristics of active materials for lead batteries

Yu. Kamenev

Scientific Research Center JSC "Electrotyaga", 50-a Kalinin str., St. Petersburg 198095, Russia

Received 16 March 2005; received in revised form 16 August 2005; accepted 26 November 2005
Available online 19 January 2006

Abstract

The individual components of electrode pastes ($4PbO{\cdot}PbSO_4$, $3PbO{\cdot}PbSO_4{\cdot}H_2O$, $PbO{\cdot}PbSO_4$) have been synthesized, their behavior has been studied during soaking and formation, and the characteristics of the active materials made of these monopastes have been determined. This approach allows purposeful optimization of electrode paste composition to meet the requirement specified for batteries.

Keywords: Lead-acid batteries; Basic lead sulphates; Processes of the soak and the formation

1. Introduction

Characteristics of active materials are determined by the composition and structure of electrode pastes, which produce these materials during oxidation (formation) and are determined by the conditions under which lead powder is mixed with acid, with subsequent soaking and electrolyte impregnation. At the time when formation starts the pastes consist of basic lead sulphates: $3PbO{\cdot}PbSO_4{\cdot}H_2O$ (3BS), $PbO{\cdot}PbSO_4$ (1BS); $PbSO_4$; lead monoxides (PbO) and metallic lead [1]. $4PbO{\cdot}PbSO_4$ (4BS) formation is also possible under certain conditions [2–4]. Thus, the active material characteristics will be determined largely by the ratio of constituents in paste, and it is very important to understand the effect of every constituent on the energy and strength characteristics of the active material. In this connection, individual components of electrode pastes (4BS, 3BS, 1BS monopastes) have been synthesized, their behavior has been studied during soaking and formation, and the characteristics of the active materials made of these monopastes have been determined. This approach allows purposeful optimization of electrode paste composition to meet the requirement specified for batteries.

E-mail address: lushina@mail.wplus.net.

0378-7753/$ – see front matter © 2005 Elsevier B.V. All rights reserved.
doi:10.1016/j.jpowsour.2005.11.098

2. Experiment results and their discussion

2.1. Synthesis of basic lead sulphates and monopaste characteristics

Monobasic lead sulphate (1BS) was prepared by the following technique. Distilled water and lead powder (degree of oxidation 70–72%) were placed in a thermally controlled mixer. Sulphuric acid having density $1.10\,g\,cm^{-3}$. The mole ratio PbO/H_2SO_4 was 2:1. The process temperature was $25 \pm 0.1\,^{\circ}C$. After acid fill the slurry was further mixed during 4 h and then filtered. The filtrate was allowed to dry at a temperature of 50–60 °C.

Tribasic lead sulphate (3BS) was prepared by using a similar technique where mole ratio PbO/H_2SO_4 was 4:1 and acid fill time was 90 min.

Tetrabasic lead sulphate (4BS) was prepared in a thermally controlled mixer. Originally, orthorhombic lead oxide (β-PbO) was thoroughly mixed with distilled water heated to 80–90 °C. Sulphuric acid having density $1.10\,g\,cm^{-3}$. The mole ratio PbO/H_2SO_4 was 5:1. After acid fill the slurry was further mixed during 3–4 h, and then filtered and allowed to dry at 100 °C. This technique is actually similar to the one employed for preparing 4BS, which was proposed in [5,6]. The technique, however, does not allow preparation of pure 4BS. To do this, the dried

filtrate was additionally heat-treated during 6 h at a temperature of 650 °C.

The average crystal sizes of 1BS, 3BS, 4BS are $(1 \div 2) \times 0.2$; $(2 \div 4) \times 0.4$ and $(20 \div 25) \times 1.8$ μm, respectively. Spatial porosity of 1BS pastes was 86%, whereas that of 3BS paste – 62% and 4BS paste – 57%. The resulting functions of pore-radius distribution for the 3BS and 4BS pastes show that they have well-defined peaks determining average pore radius 2000 and 5700 Å, respectively. The findings agree with the results of [2,3,8].

2.2. Sulphation (soaking) of basic lead sulphates

To study the sulphation process, use was made of basic lead sulpfates (*n*-BS) powders and plates covered with the pastes made of the same salts. The maximum size of powder particles was 40 μm, whereas the plate size was $60 \times 45 \times 3$ mm. The *n*-BS reactivity was determined by the following technique. The *n*-BS powder was poured into acid solution being thoroughly mixed. In certain time periods the slurry was rapidly placed on the filter and washed with distilled water. The resulting sediment was analyzed for $PbSO_4$. Powder testing made it possible to avoid the effect of structural characteristics of pasted plates. The sulphation process was studied by keeping the plates in a thermally controlled cell that was filled with water and by analyzing the pastes for sulphate content. Furthermore, the paste phase composition was determined by using the X-ray phase technique, whereas the paste structure was determined with the use of electron microscope. The sulphation process was studied over the temperature ranges of 20–50 °C, with 1.05–1.25 g cm^{-3} acid density and 0–8 h stand time.

In general, the sulphation process can be represented by diagram [7]:

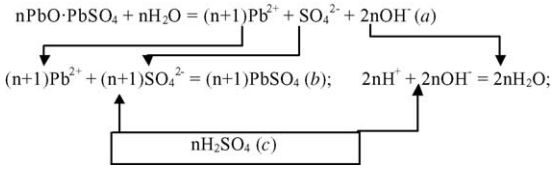

(1)

Fig. 1 shows variations in the phase compositions of 3BS and 4BS pastes during sulphation as based on X-ray phase analysis. Similar methods were used in [7–9]. Similar results may not be obtained for 1BS pastes because of their rapid shedding from the grids in filling the plate pores with acid. It has been shown that, in soaking, only $PbSO_4$ occurred on the plate surface, which corresponds to diagram (1). At the same time, internal paste layers contained during sulphation not only $PbSO_4$, but also 1BS (soaking of 3BS) and 3BS, 1BS (soaking of 4BS) the quantity of which initially increased and then decreased. It is apparent that the mechanism of sulphation in accordance with diagram (1) can be implemented only where there is surplus acid. Under real plate soaking conditions, however, the reaction zone becomes acid-depleted and a stoichiometric correspondence between Pb^{2+} concentration (stage a) and SO_4^{2-} concentration (stage c) is violated in this zone. Such depletion may be due to both sulphation reactions proper and formation on the surface of *n*-BS crystals of $PbSO_4$ layer preventing the acid from being transferred to reaction zones. Fig. 2 clearly shows formation on 3BS and 4BS surface of the primary $PbSO_4$ fine-grained layer that densely covers the large *n*-BS prismatic crystals. Sulphation reactions under SO_4^{2-} deficiency will

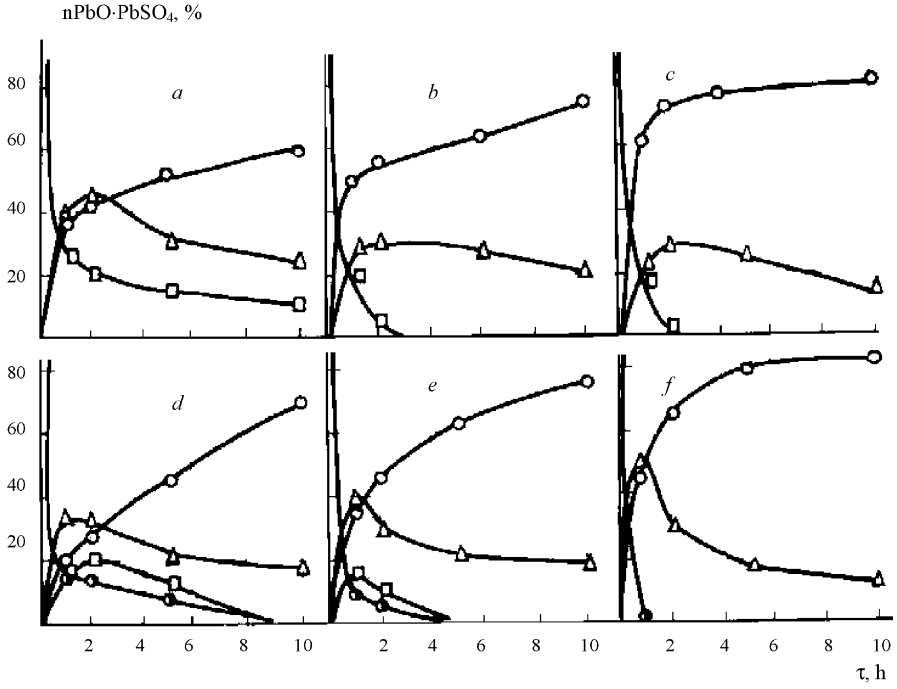

Fig. 1. Relationship for compositional variations in the 3BS (a–c) and 4BS (d–f) pastes during acid soaking at a density of (g cm^{-3}): 1.05 (a and d), 1.10 (b and e), 1.25 (c and f); 4BS (◑), 3BS (□), 1BS (△), $PbSO_4$ (◯).

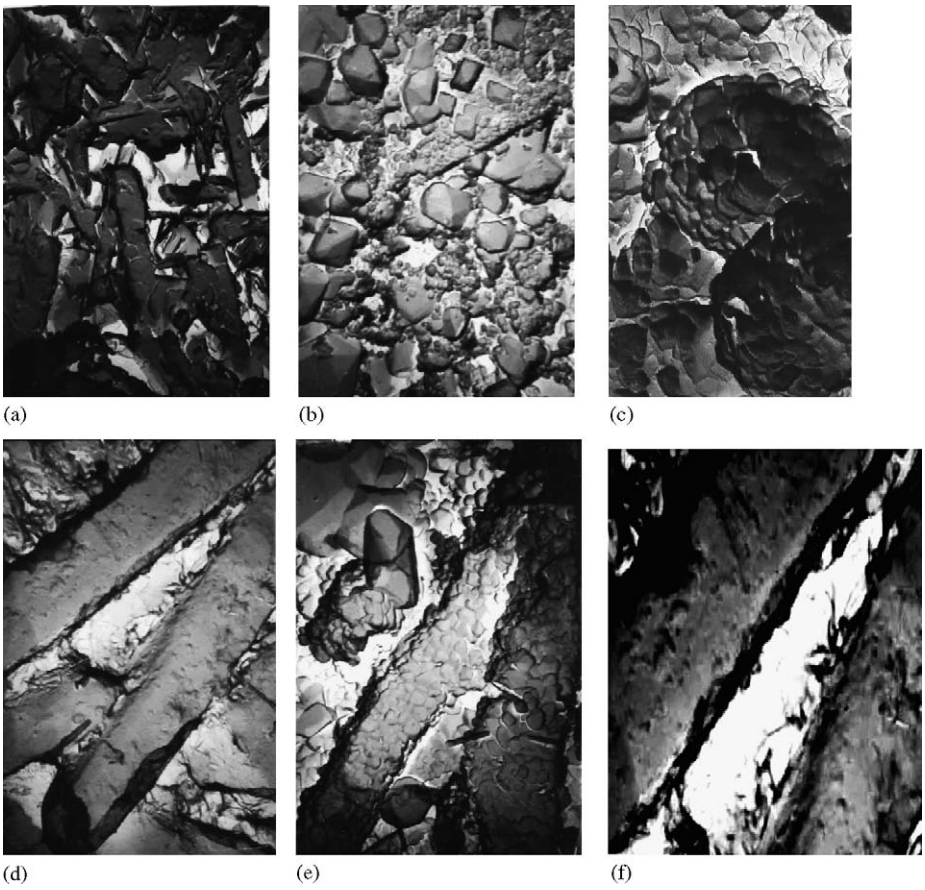

Fig. 2. Surface structure of plates made of 3BS (a–c) and 4BS (d–f) pastes prior to formation (a and d), subsequent to soaking (b and e), and at the end of formation (c and f). Magnification: 10,000×.

proceed not until $PbSO_4$ formation, but until *n*-BS formation, with *n*-BS having lower basic capacity than the original sulphate. For 3BS, the real sulphation diagram can then be written as:

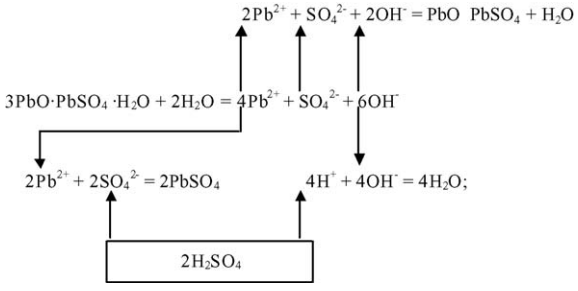

(2)

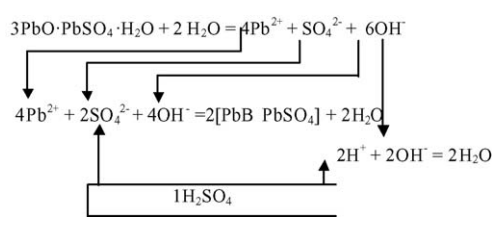

(3)

For 4BS, sulphation diagrams can be written as:

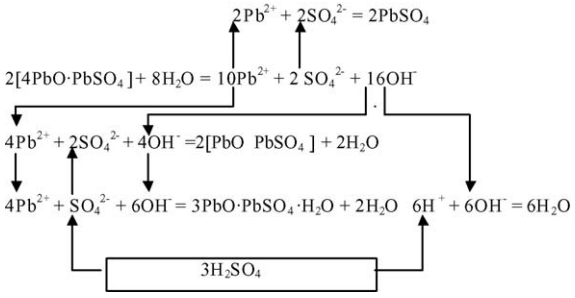

(4)

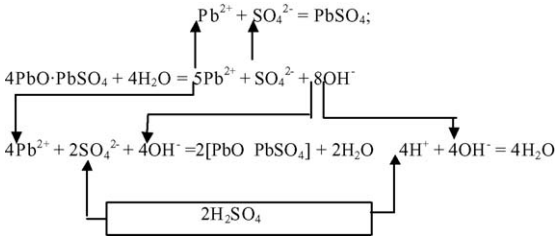

(5)

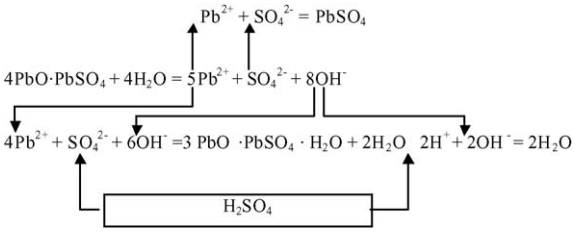

(6)

In the further soaking and acid diffusion, the newly formed *n*-BS undergo further sulphation with a decrease in their basic capacity, as demonstrated by the paste analysis results that are shown in Fig. 1. But even after prolonged soaking the *n*-BS still remain under the dense layer of $PbSO_4$, which determines largely the pre-formation paste structure.

The analysis of soaking time-dependent variations in the sulphation degree of 1BS, 3BS, 4BS powders shows that the sulphation degree ratio of 1BS/3BS/4BS powders was approximately 4.5/3.5/1. With a knowledge of the average sizes of salt crystals and their density [10], it is possible to determine the ratio of *n*-BS-specific area surfaces which is ~4.5/4.0/1. Thus, it is clear that the *n*-BS sulphation degree is primarily determined by their specific surface area.

In soaking the plates made of the 3BS and 4BS pastes, their sulphation degree ratio is ~3/1. It can be shown that here the sulphation degree is determined by the surface of pastes in the plate. It has been found that the pore radius distribution function for the 3BS and 4BS pastes has a distinct maximum, which allows the porous plate model to be viewed as the model of capillary pores having a constant radius. The internal surface of plates (S) can then be written as:

$$S = 2\pi N r \beta \delta, \tag{7}$$

where N is a number of pore orifices per unit surface, r an average pore radius, β the pore twisting, and δ is the plate thickness. It is not feasible to determine experimentally N and β. But since the volume porosity (γ) of the model being studied is

$$\gamma = \pi N r^2 \beta,$$

then

$$N\beta = \frac{\gamma}{\pi N r^2}$$

we have

$$S = \frac{2\gamma\delta}{r} \tag{8}$$

where the parameters can all be readily determined from experiments. Substituting the known values into Eq. (8) shows that $S_{3BS}/S_{4BS} = 3.2$, which corresponds to the sulphation degree ratio for the salts being studied.

It has been found that, in the extreme case, the *n*-BS sulphation degree depends on acid density and has a maximum around 1.05–1.40 g cm^{-3}. This is because, on the one hand, an increase in acid concentration increases the rate of sulphation reaction in accordance with the law of chemical kinetics, but, on the other hand, it impedes the reaction as a result of formation of dense sulphate sediments. It is significant that at the initial soaking time, when the sulphate layer has not been formed, the sulphation rate continuously increases with an increase in acid concentration.

The sulphation rate increases with an increase in temperature, which is due to its effect on the rate of chemical processes, a decrease in acid viscosity and fuller acid fill of plate pores. Furthermore, an increase in temperature leads to the formation of a larger coarse-grained layer of $PbSO_4$ having a higher porosity.

2.3. Formation of basic lead sulphates

A general reaction for *n*-BS formation can be represented as:

$$\begin{aligned} &n\mathrm{PbO}\cdot\mathrm{PbSO_4} + \gamma_1\mathrm{H_2O} = \gamma_2\mathrm{Pb^{2+}} + \gamma_3\mathrm{OH^-} + \mathrm{SO_4^{2-}}(a)\\ &\gamma_5\mathrm{Pb^{2+}} + 2\gamma_5\mathrm{H_2O} = \gamma_5\mathrm{PbO_2} + 4\gamma_5\mathrm{H^+}(b)\\ &(\gamma_2-\gamma_5)\mathrm{Pb^{2+}} + (\gamma_2-\gamma_5)\mathrm{SO_4}^{2-} = (\gamma_2-\gamma_5)\mathrm{PbSO_4}(c) \end{aligned} \tag{9}$$

where $n = 0, 1, 3, 4$ is basic capacity of salt; γ_i is stoichiometric coefficient.

The active material formation current can be described by the kinetic equation:

$$I_{\mathrm{AM}} = k\Theta_1 a_{\mathrm{Pb}(\Pi)} \exp\left(-\frac{W_\mathrm{a}}{RT}\right) \tag{10}$$

where $a_{\mathrm{Pb}(\Pi)}$ is activity of Pb^{2+} ions, Θ_1 the surface on which process (b) is implemented, k the rate constant and W_a is process activation energy.

The activity of lead ions in Eq. (10) is determined, on the one hand, by the heterogeneous dissolution of *n*-BS (a), and, on the other hand, by the rate of sulphation reaction (c) which proceeds to form difficult-to-solve $PbSO_4$ salt. Then:

$$\Theta_1 + \Theta_2 + \Theta_3 = 1 \tag{11}$$

$$\frac{\mathrm{d}a_{\mathrm{Pb}(\Pi)}}{\mathrm{d}\tau} = k_\mathrm{p}\Theta_2 + k_\mathrm{pp}\Theta_3 - k_0 a_{\mathrm{SO_4}} a_{\mathrm{Pb}(\Pi)} \tag{12}$$

where k_p, k_pp, Θ_2, Θ_3 and k_p, k_pp, Θ_2, Θ_3 are specific rates of solution and surfaces for nPbO·$PbSO_4$ and $PbSO_4$, respectively; k_0 the constant of $PbSO_4$ formation rate and $a_{\mathrm{SO_4}}$ is the activity of sulphates of ions. It is apparent that Θ_1,Θ_2, Θ_3, $a_{\mathrm{SO_4}}$ are time-dependent. In the initial period of formation, the Θ_1 value is equal to the current tap surface and increases as PbO_2 forms. The Θ_2 value decreases during formation because the *n*-BS salt surface is replaced by the $PbSO_4$ (Θ_3) surface as a result of sulphation reaction. The activity of sulphate ions is determined by the rate relationship of electrochemical and chemical reactions, and by the diffusion conditions concerning structural transformations in the paste. The solution of differential Eq. (10) under the initial condition $\tau = 0$, $a_{\mathrm{Pb}(\Pi)} = 0$, is an equation of the form:

$$a_{\mathrm{Pb}(\Pi)} = \exp\left(-k_0\int_0^\tau a_{\mathrm{SO_4}}\,\mathrm{d}\tau\right) \times \left[\int_o^\tau (k_\mathrm{P}\Theta_2 + k_\mathrm{pp}\Theta_3)\exp\left(k_0\int_o^\tau a_{\mathrm{SO_4}}\,\mathrm{d}\tau\right)\mathrm{d}\tau\right] \tag{13}$$

Introducing additional conditions we may simplify Eq. (13). Obviously, in the initial period it is possible to assume that

Table 1
Output of current vs. oxidation potential

Monopaste	Output of current (%)				
	$E = 1100$ mV	$E = 1200$ mV	$E = 1300$ mV	$E = 1400$ mV	$E = 1500$ mV
3BS	87.1	97.0	75.0	62.1	42.8
4BS	83.9	99.2	75.2	36.5	22.6

$\Theta_2 + \Theta_3 \gg \Theta_1$, and then $\Theta_3 = 1 - \Theta_2$. Variations in Θ_3 over time can be described by a power series. Restricting ourselves to the first three terms and considering that $(\Theta_3)_{\tau=0} = 0$ we get

$$\Theta_3 = n_1\tau + n_2\tau^2 \tag{14}$$

After performing the relevant operations we may transform Eq. (13) to the form:

$$a_{\mathrm{Pb}(\Pi)} = \frac{k_{\mathrm{pp}} - k_{\mathrm{p}}}{k_0 a_{\mathrm{SO_4}}(\tau)}(n_2\tau^2 - k_0 a_{\mathrm{SO_4}}(\tau)\tau) \tag{15}$$

where $a_{\mathrm{SO_4}}(\tau)$ is an $a_{\mathrm{SO_4}}$ value at an instant of time in the (0, τ) interval and n_2 is the coefficient of power series (Eq. (14)). It follows from Eq. (15) that the activity of lead ions decreases with τ increasing. Physically, the resulting solution means that a decrease in Pb^{2+} activity is due to the replacement during formation of the surface of easy-to-solve *n*-BS salts by the surface of difficult-to-solve $PbSO_4$. This implies an important recommendation that formation has to be carried out under conditions of minimum rate of plate sulphation, which will allow acceleration of paste oxidation.

The *n*-BS paste formation was examined under the conditions of controlled potential and galvanostatic polarization in order to study the mechanism of paste oxidation and optimize the process variables. The controlled potential study shows that the beginning of paste oxidation, which is shown by the $(I-\tau)_\varphi$ current–time curves and determined by a current increase, corresponds to the 1100 mV potential (here, and in what follows, potentials are given in terms of Hg/Hg_2SO_4 of reference electrode). With this potential, the external corrosion layer at the current grid/paste boundary, which consists of $PbSO_4$ (an equilibrium potential of $PbSO_4 \leftrightarrow PbO_2$ process is ~1100 mV) oxidizes into the conducting PbO_2, which ensures an electrical contact between the paste and the grid. It is significant that the $(I-\tau)_{\varphi=1100}$ curves exhibit a small current peak preceding the current increase which is absent on the curves taken for potentials below 1100 mV where there is no current increase due to paste oxidation. Given below is the relationship between the paste formation output of current (%) and potential (E) for 3BS and 4BS (Table 1), which was determined as a ratio of the amount of electricity used to form PbO_2 and calculated by the paste analysis result for the PbO_2 content to the total amount of electricity that had passed during the formation process.

The maximum output of current corresponds to the 1200 mV oxidation potential. An increase in the potential increases the rate of water decomposition, which leads to a reduction in the formation output of current.

Fig. 3 shows the $(I-\tau)_\varphi$ curves taken for 3BS and 4BS with 1100–1600 mV potentials. A wide maximum of current can be seen on these curves. The initial current increase involves: (1) an increase in the PbO_2 (Θ_1) surface and formation development throughout the plates; (2) a high concentration of $a_{\mathrm{SO_4}}$ due to a high concentration of $a_{\mathrm{Pb}(\Pi)}$; (3) a decrease in the $a_{\mathrm{SO_4}}$ concentration due to sulphation reactions; (4) formation of PbO_2 having a smaller specific volume than $PbSO_4$ and facilitation of acid access to the *n*-BS that are blocked by $PbSO_4$ crystals. Increasing the peak height with an increase in the oxidation potential is determined by an increase in the oxidation rate of lead ions. According to the authors [11–13], the current drop on the $(I-\tau)_\varphi$ curves is due to a decrease in the quantity of unformed pastes. This paper, however, shows that the PbO_2 content at the current peak for the 3BS and 4BS plates is 10–11 and 3–5%, respectively. The current drop may be thought of as being due to a reduction of the surface of easy-to-solve *n*-BS (Θ_3) to the surface of difficult-to-solve $PbSO_4$ (Θ_2), which, in accordance with (21), reduces $a_{\mathrm{Pb}(\Pi)}$ and the rate of paste oxidation. The current peak on the $(I-\tau)_\varphi$ curves for 4BS pastes is narrower than that for 3BS. Obviously, the coarse-grained structure of 4BS pastes has a smaller surface than 3BS and reduces the time required for replacement of Θ_3 by Θ_2. From Fig. 3 it can be seen that the formation rate of 3BS is significantly higher than that of 4BS, which is also due to the inequality, $\Theta_3 < \Theta_2$. An increase in current for the 4BS pastes occurs after the peak. Its occurrence is due to water oxidation because of an increase in the reaction surface (PbO_2). The absence of the second increase in the current for 3BS is due to the fact that the current increase involved in water decomposition may not offset the current drop involved in a decrease of the 3BS oxidation rate. After a certain controlled potential polarization period the magnitude of current becomes stabilized and corresponds to the water oxidation rate under the conditions of constant potential and reaction surface (PbO_2).

From the above discussion, it follows that chemical reactions of sulphation have a profound effect on the rate of paste oxidation. Fig. 4 shows that oxidation current decreases with an increase in pre-formation soaking time under controlled potential polarization. There is also a decrease in the peak value of current on dynamic potential cathode curves involved in the reduction of PbO_2 formed during anode polarization, which also indicates that the efficiency of paste oxidation decreases with an increase in soaking time.

To optimize the parameters of paste formation, 3BS and 4BS plates were manufactured. The plate size was $60 \times 40 \times 3$ mm. The plates were placed in thermostatically controlled cells with two negative plates and galvanostatically formed. The process was conducted over the following ranges of process variables: temperature of 20–50 °C, H_2SO_4 density of 1.05–1.25 g cm^{-3}, current density of 0.25–2.00 A dm^{-2}, soaking time of 0–8 h. In

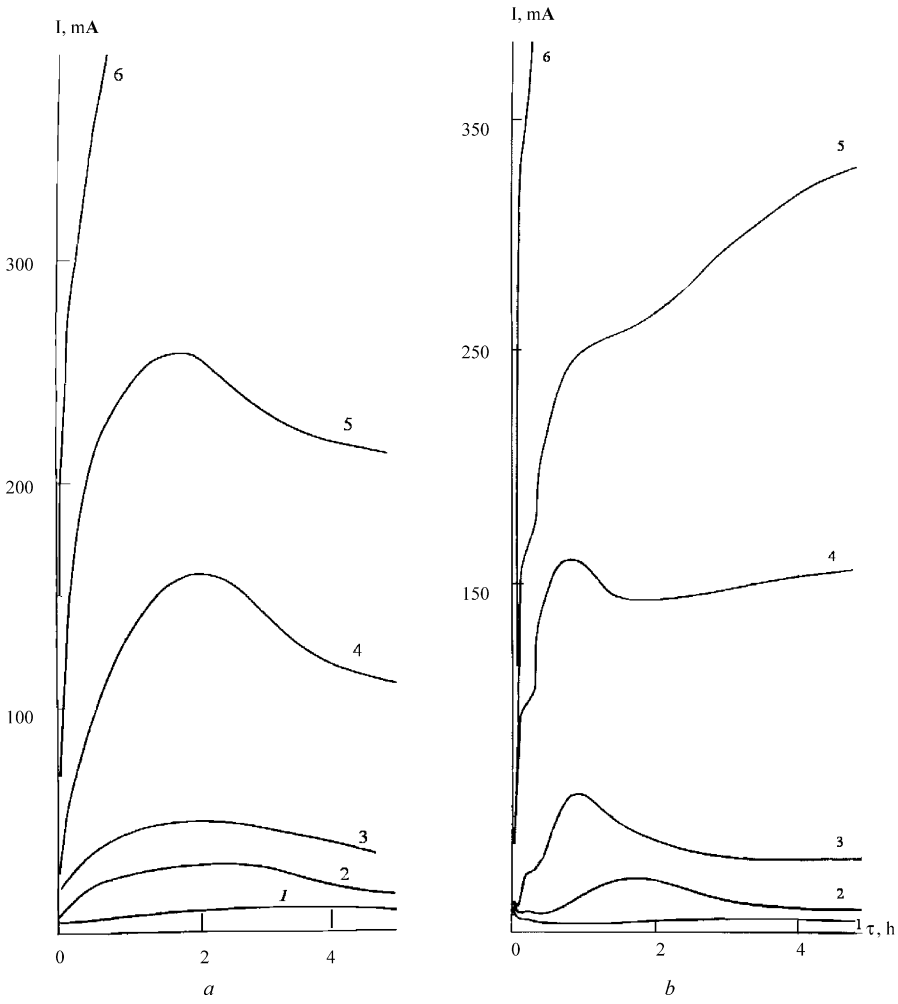

Fig. 3. Curves $(i-\tau)_{\varphi}$ taken at constant potentials, V: 1.10 (1), 1.20 (2), 1.30 (3), 1.40 (4), 1.50 (5) and 1.60 (6) for plates made of 3BS (a) and 4BS (b) pates.

formation, the PbO_2, $PbSO_4$ content in the plates being formed, phase composition and structure were determined in 1, 3, 5, 10 and 15 h. Experimental results are shown in Fig. 5. From Fig. 5 it can be seen that: (1) most curves $PbO_2 = f(\tau)$ have two regions — the region of rapid PbO_2 accumulation, the slope of which depends on formation conditions, and the region of slow PbO_2 accumulation, the slope of which is hardly dependent on formation conditions; (2) the rate of plate formation is the lowest one under most favorable conditions for sulphation processes (under these conditions a degeneracy is observed in the first region of curves $PbO_2 = f(\tau)$); (3) the rate of 4BS paste formation is initially higher than that of 3BS pastes, although 3BS oxidation was more rapid at a later time. These patterns can all be explained from the formation mechanism described by diagram (9) and equations [14,15]. It is apparent that the first region of curves $PbO_2 = f(\tau)$ captures the oxidation process under conditions of high Pb(Π) concentration because of high *n*-BS dissolution rate, $(\Theta_2 > \Theta_3)$, which depends on formation conditions. In the second region, where $\Theta_2 = 0$, the Pb(Π) concentration is determined by $PbSO_4$ solubility which is low and little dependent on formation conditions. It can be seen from the curves $PbSO_4 = f(\tau)$ that durations of paste sulphation for the first region $PbO_2 = f(\tau)$ are also the same and are about 5 h. Thus, completion of plate sulphation leads to a considerable reduction in the rate of paste oxidation. This idea is most clearly illustrated by Fig. 5 h, h′. From this figure it can be seen that the longer is the preliminary sulphation duration, the smaller is the slope of curve $PbO_2 = f(\tau)$, and for 8 h soaking time the slope of this curve corresponds to that of curve $PbSO_4 = f(\tau)$ from the very beginning of oxidation.

From the above discussion it follows that, to accelerate the formation process, it has to be conducted under conditions of lowest sulphation rate and minimum time of preliminary soaking.

Fig. 2 shows structural variations in the electrode pastes made of 3BS and 4BS during their formation. From this figure it can also be seen that the coarse-grained structure of 4BS is retained by the active material structure (metasomatic effect), whereas the prismatic structure of 3BS is transformed into a spherical structure. Thus, the 4BS active materials are characterized by the presence of the space framework formed by PbO_2 prismatic blocks, and we may expect an improvement in its strength during cycling and an increase in the life of batteries having such an active material [14–17].

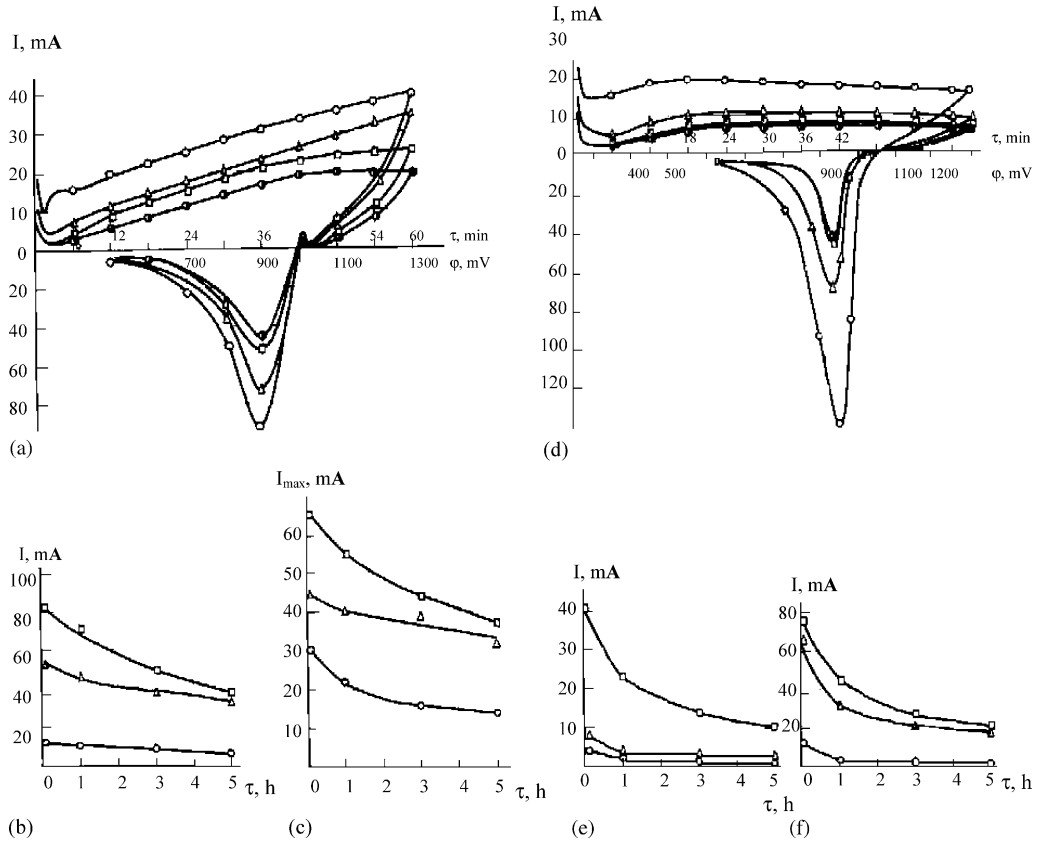

Fig. 4. Controlled potential anode curves obtained at 1.30 V potential and dynamic potential cathode curves taken after 1 h polarization at 1.30 V for plates made of 3BS (a) and 4BS (d) pastes. Soaking time duration (h): 0 (◯), 1 (△), 3 (□), 8 (◑). Current at the end of 1 h polarization with potentials, V: 1.20 (◯), 1.30 (△), 1.40 (□) for 3BS (e) and 4BS (b) vs. preliminary acid soaking time. Amount of cathode peak on $i - \tau$ curves subsequent to controlled potential polarization with potentials, V: 1.20 (◯), 1.30 (△), 1.40 (□) for plates made of 3BS (f) and 4BS (c) pastes vs. preliminary acid soaking time.

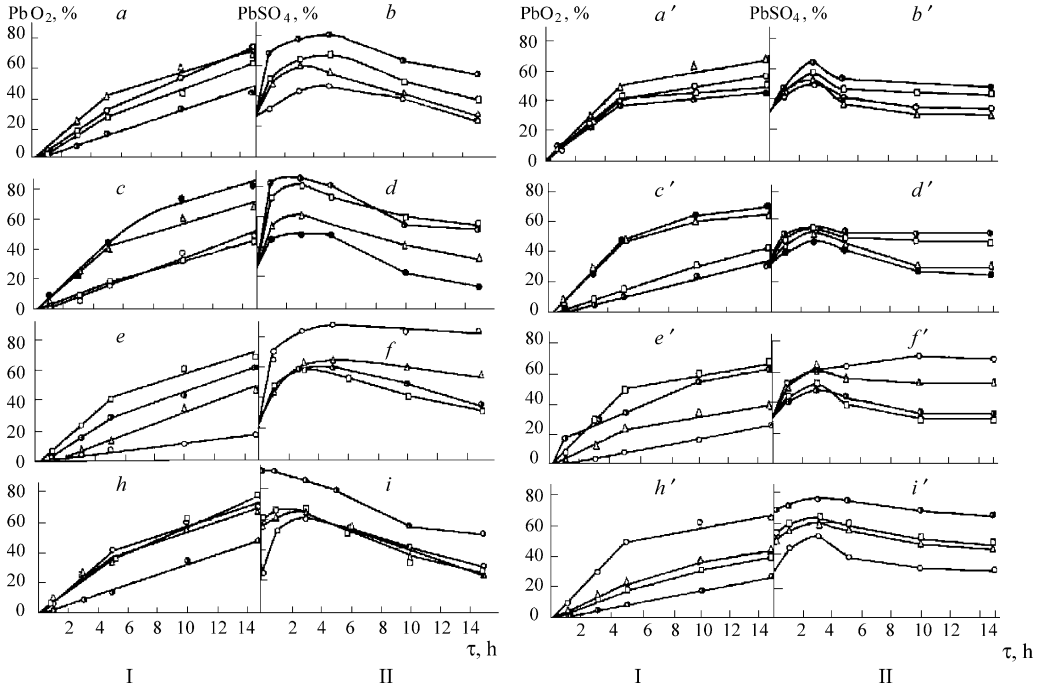

Fig. 5. Variations in the PbO_2(I) and $PbSO_4$(II) content during formation of 3BS (a–i) and 4BS (a′–i′) pastes. Formation conditions: a, b, a′, b′ — current density 1.0 A dm^{-2}, electrolyte density 1.10 g cm^{-3}; soaking time 0 h; temperature (°C): 20 (◯), 30 (△), 40 (□) and 50 (◑); c, d, c′, d′ — current density 1.0 A dm^{-2}; soaking time 0 h; temperature of 30 °C, electrolyte density (g cm^{-3}): 1.05 (●), 1.10 (△), 1.15 (□) and 1.25 (◑); e, f, e′, f′ — soaking time 0 h; temperature of 30 °C, electrolyte density 1.10 g cm^{-3}, current density (A dm^{-2}): 0.25 (◯), 0.5 (△), 1.0 (□) and 2.0 (◑); h, i, h′, I′ — current density 1.0 A dm^{-2}; temperature of 30 °C, electrolyte density 1.05 g cm^{-3}; soaking time (h): 0 (◯), 1 (△), 3 (□) and 8 (◑).

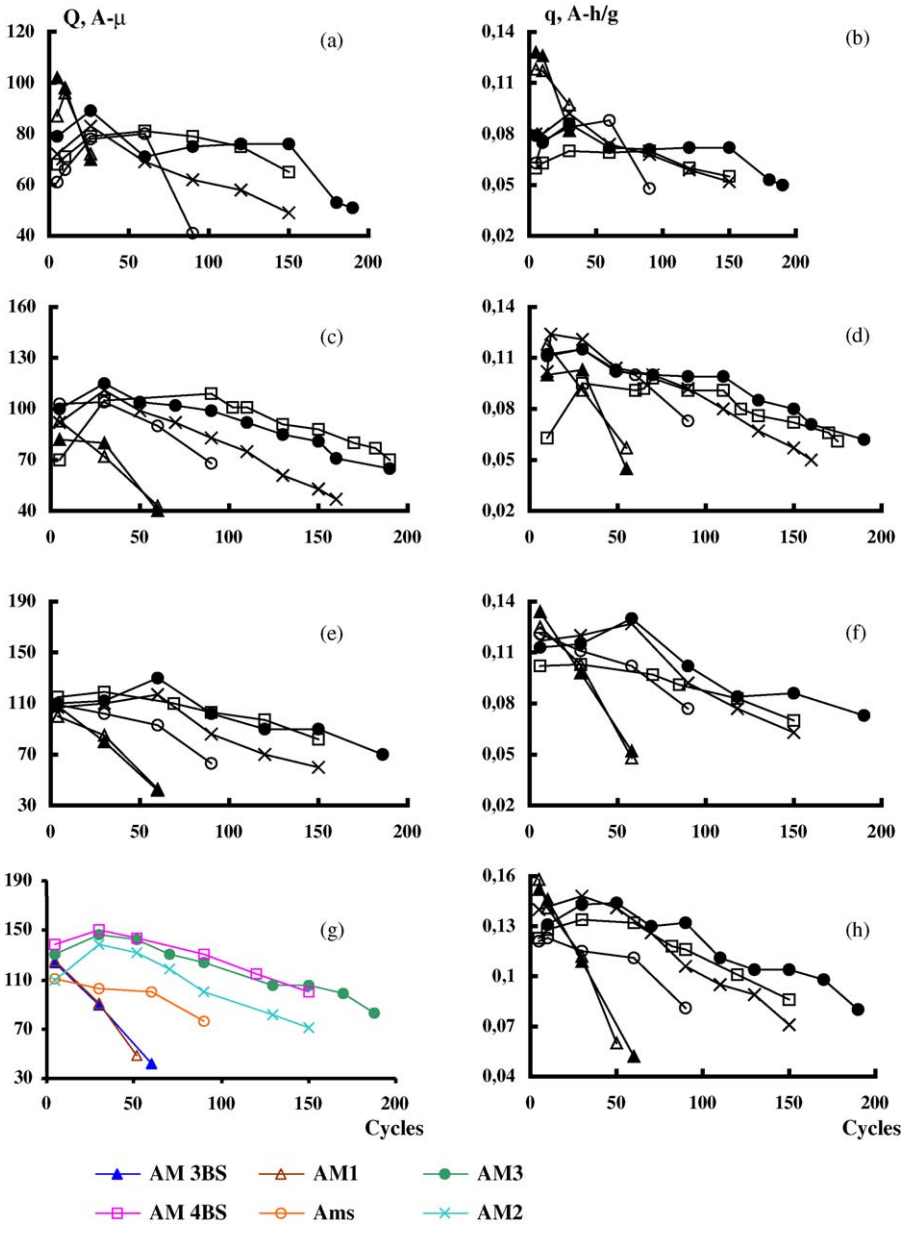

Fig. 6. Actual capacity (Q) and capacity related to unit weight of lead in paste (q) vs. number of cycles. Discharge duty: 1 h duty — a, b; 5 h duty — c, d; 10 h duty — e, f; 50 h duty — h, i.

2.4. Electrical and life characteristics of test active materials

To estimate electrical and life characteristics of active materials made of 3BS and 4BS, the 12 V and 140 Ah batteries with such active materials were manufactured and tested. Fig. 6 and Table 2 show the test results for batteries with test and series active materials. It follows from the table that the active materials made of 3BS (AM_{3BS}) had specific electrical characteristics and active material utilization factors (AMUF) superior to similar parameters of series (AM_S) active materials and 4BS (AM_{4BS}) active materials. In this case, however, the life of batteries with AM_{3BS} was very short. The AM_{4BS} batteries had lower electrical characteristics than series batteries, but their life was 1.8 or 2.0 times longer [3,16,17]. These patterns are related to structural features of active materials. On the one hand, the coarse-grained nature of AM_{4BS} structure favors formation of strong framework that ensures a longer service life, while on the other hand, their small specific surface area reduces specific capacity characteristics. Conversely, the developed AM_{3BS} surface ensures high specific characteristics but has no service life because of its sagging. The results we have obtained show that 3BS and 4BS active materials have good prospects. Large-size crystals AM_{4BS} in such active materials will form a space framework to ensure a stable operation of high-capacity AM_{3BS}.

The active materials ($AM_{3BS} + AM_{4BS}$) can be produced by three techniques:

1. mechanical mixing of separately synthesized 3BS and 4BS and their formation (AM1);

Table 2
Test results for batteries with test active materials

Discharge duty (h)	Paste for preparing active materials					
	Series		3BS		4BS	
	Specific capacity (Ah g^{-1})	AMUF (%)	Specific capacity (Ah g^{-1})	AMUF (%)	Specific capacity (Ah g^{-1})	AMUF (%)
1	0.08	30.7	0.142	53.0	0.059	22.8
10	0.151	57.8	0.187	70.0	0.122	47.3

2. direct synthesis of 3BS and 4BS in reactor and their formation (AM2);
3. high temperature treatment of series pastes and their formation (AM3).

The last technique is based on the fact that, when heated, 3BS is decomposed into a mixture of 4BS and 1BS [6]. In this work, the series pastes made of 3BS, 1BS and α-PbO were heated. Fig. 7 shows a temperature–time region for stable 4BS formation. In this region, the pastes consisted mainly of 4BS, α-PbO, β-PbO. The material obtained was mechanically comminuted and mixed with water to obtain the required viscosity for making the paste.

The 12 V and 140 Ah batteries with AM1, AM2 and AM3 test pastes were manufactured. The alloy Pb–2.5% Sb–1.2% Sn was used for making grids. The AM1 paste was prepared by forming the mechanical 90% 3BS and 10% 4BS mixture; the AM2 paste was prepared by forming the paste synthesized at a temperature of 80 °C by mixing PbO and H_2SO_4 and containing 3BS, 4BS and 1BS; the AM3 paste was prepared by forming the series paste (post-treatment composition of 4BS, β-PbO) subjected to 2 h heat treatment at 650 °C. Further additives were not introduced into the positively active mass.

The cycling results (Fig. 7) show that the AM1 batteries have characteristics that are similar to those of AM_{3BS} batteries, which indicates that the mechanical *n*-BS mixture containing a small quantity of 4BS is inefficient. The strengthening effect was achieved with the 4BS 50–60% content, although specific electrical characteristics were not high. Thus, the mechanical mixture is unable to create the strengthening framework during formation to allow the efficient utilization of AM_{3BS} capacity. On the other hand, even a small quantity of 4BS in the paste produced by the second technique makes it possible to produce high-strength and energy-intensive active materials having the service life at the AM_{4BS} level. Finally, the AM3 batteries exhibit the best energy and life characteristics.

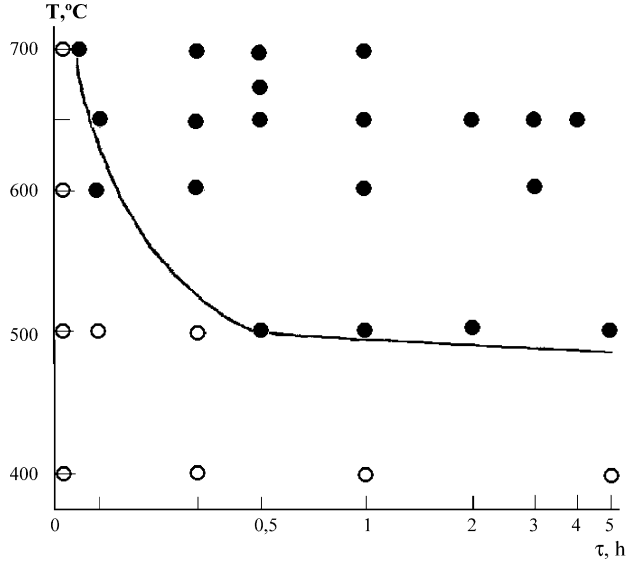

Fig. 7. Temperature–time region of 4BS formation. Pastes containing 4BS (●) and containing no 4BS (◯).

3. Conclusions

This work has identified the mechanism of *n*-BS sulphation and shown the effect of basic process variables on the kinetics of this process.

The mechanism of paste formation has been studied and a significant effect of chemical reactions of sulphation on its kinetics has been first shown. Based on the developed formation mechanism, the principle for its organization has been provided and basic process variables have been optimized.

Discharge characteristics of active materials made of individual electrode paste constituents have been studied. The role of each constituent has been shown and recommendations have been given for the paste composition to ensure, along with high-energy characteristics, an increase in the service life of battery 1.8 or 2.0 times. The use of such active materials makes it possible to avoid the utilization of polymer strengthening additives whose application is extremely undesirable in sealed batteries and will ensure prolonged service life.

References

[1] A.I. Rusin, Modern Technology of Lead-Acid Batteries, Energiya, Leningrad, 1987, p. 182.
[2] D. Pavlov, G. Papazov, J. Appl. Electrochem. 4 (4) (1976) 339–345.
[3] S. Grugeon-Dewaele, J.B. Leriche, J.M. Tarascon, J. Power Sources 64 (1997) 71–80.
[4] W.R. Kitchens, R.G. Osten, D.W.H. Lambert, J. Power Sources 53 (1995) 263–267.
[5] J. Burbank, J. Electrochem. Soc. 113 (1) (1966) 14–18.
[6] R.F. Dapo, J. Electrochem. Soc. 121 (2) (1974) 72–76.
[7] D. Pavlov, G. Papazov, V. Iliev, J. Electrochem. Soc. 119 (1) (1972) 8–19.
[8] D. Pavlov, G. Papazov, V, Iliev Sbornik rabot po istothn, Toka, 1984, Leningrad, pp. 18–23.
[9] F.B. Diniz, L. Borges, Proceedings of the International Conference on Lead-Acid Batteries LABAT'99, Bulgaria, 7–10 June, 1999, pp. 151–153.
[10] M.A. Dasoyan, I.A. Aguf, Contemporary Theory of Lead-Acid Batteries, Energiya, Leningrad, 1975, p. 272.

[11] E.L. Lawrence, R.I. Ball, R. Evans, R. Stevens, J. Power Sources 110 (2002) 125–132.
[12] A.F. Bodenschutz, Electrochim. Acta 13 (10) (1968) 2013–2019.
[13] E. Skoluda, Electrochim. Acta 19 (6) (1974) 235–238.
[14] J.E. Manders, L. Lam, K. Peters, R. Prengaman, J. Power Sources 59 (1996) 199–207.
[15] D. Pavlov, J. Power Sources 53 (1996) 9–21.
[16] D. Pavlov, G. Papazov, B. Manahov, Proceedings of the International Conference on Lead-Acid Batteries LABAT'99, Bulgaria, 7–10 June, 1999, pp. 75–81.
[17] N. Saidi, H. Saidi, B. Saidani, S.P. Stoylov, J. Power Sources 64 (1997) 61–64.